scientific reports

Check for updates

OPEN

Experimental results of a 330 GW impedance-matched Marx generator

Vahid Damideh[1,2]✉, J. C. Btaiche[1,2], Alex Ho[1,2], R. B. Spielman[3], Jane M. Lehr[1,2,5], T. A. Mehlhorn[1,2,4], Isaac Hassen[2], Alexei Akoulov[2], Elahe Aranfar[2], Alex McDonald[5], Pierre Tochon[2], Ayan Choudhury[2], Emile Beaulieu[2], Hao Xian Tan[2], Anson Yu[2], Sophie Faliero[1], Richard Tetreault[2], Gael Breault[2], Rodrigue Tetreault[2], Negar Hosseiny[2] & Edward Smith[2]

Impedance-matched Marx generators (IMGs) are considered next generation pulsed-power drivers because of their long lifetime (> 10,000 shots), repetition rate (> 0.1-Hz), fast rise time (~ 100-ns), and high-energy-delivery efficiency (~ 90%). "TITAN" is a 14-stage IMG designed to deliver 1-TW to a 2-Ω matched load. In this paper, design, simulation, and experimental results for six stages of TITAN including its triggering system, air delivery system, and pulse shaping are presented. To achieve efficiency over 85% and maximize the capability of an IMG, synchronized triggering, reduced pre-fire rate, and pulse shaping ability are crucial. In this paper, novel engineering solutions are introduced, tested, and proven to overcome those challenges. 6-stage TITAN, powered by 102 identical bricks and 102 field-distortion-triggered gas switches, could generate ~ 600-kA and ~ 700-kV across a ~ 0.9-Ω matched load when fully charged to ± 100-kV. In these experiments, 6-stage TITAN is tested up to ± 70-kV charge voltage which delivers a peak power of 330-GW to a 1.2-Ω resistive load.

Keywords TITAN, Impedance-matched Marx generator (IMG), Next-generation pulsed-power (NGPP), Z-pinch, Magnetically driven inertial fusion, Z pulsed-power accelerator

The evolution of pulsed-power drivers for fusion-related applications has been a subject of significant research and development in the last few decades. Various technologies, such as linear transformer drivers (LTDs)[1–4] and impedance-matched Marx generators (IMGs)[1–5], have been introduced to address the need for pulsed, magnetized-plasma fusion approaches[6–10] and next-generation, pulsed-power (NGPP) facilities[11–14]. The characteristics required for pulsed-power drivers include fast rise time (~ 100-ns), high current (> 1-MA), high voltage (> 1-MV), high efficiency (> 85%), and repetition rate (> 0.1-Hz)[15]. While conventional fast discharge capacitor banks have been used in devices that drive dense plasma focuses and Z-pinches[16–22], they have limitations in achieving the high voltage and short rise time necessary for pulsed fusion approaches and NGPP facilities. Recent Marx generator technologies have been able to produce higher voltages with a faster rise time than conventional capacitor banks, however, the high voltages and currents present in the latest stages (peaking/steepening switches) of the generators result in short switch lifetimes[23]. To achieve even faster rise times using Marx generators, they need to be equipped with a pulse forming line (PFL) like the Z pulsed-power facility at Sandia National Laboratories (SNL)[24]. In this case, the efficiency of the pulsed-power facility using a Marx Generator with a PFL is half (~ 50%) of IMG-based facilities, and its components have shorter lifetimes[14,23]. IMG-based facilities double (2x) the energy efficiency of traditional Marx generators coupled to a PFL.

LTD is a technology that uses low-capacitance, low-inductance components, and low-jitter switches that achieve a rise time of the output pulse in the order of 100-ns or even faster. However, LTDs have high cost, complexity, weight, and triggering challenges at large fusion facilities[14]. To overcome these disadvantages, IMGs have been introduced as a new class of pulsed-power drivers. An IMG is less expensive and slightly more efficient than an LTD for a given electrical-power output time histogram, as it does not use ferromagnetic cores and does not have significant triggering issues[1,2].

[1]Fuse Energy Technologies Corp., San Leandro, CA, USA. [2]Fuse Energy Technologies Inc., Napierville, QC, Canada. [3]Laboratory for Laser Energetics, University of Rochester, Rochester, NY, USA. [4]Department of Nuclear Engineering and Radiological Sciences, University of Michigan, Ann Arbor, MI, USA. [5]Department of Electrical and Computer Engineering, University of New Mexico, Albuquerque, NM, USA. ✉email: vahid@f.energy

The recent developments in fusion-oriented pulsed-power modules, such as the LTD-based M-50 testbed[25] and the Marx generators with PFLs in the Z pulsed-power facility at SNL[8], reflect the ongoing efforts to advance pulsed-power technology for fusion-related applications.

IMGs are the most advanced pulsed-power drivers and are being considered for the NGPP facilities[1,2], pulsed-power accelerators[26], flash x-ray and gamma-ray sources[26–29], high-energy lasers (HEL)[30], high-power microwaves (HPM)[31,32], excimer lasers[30], materials under extreme conditions[33,34], high-energy density plasmas[12,35–37], radiation and nuclear effects[26,38], national security research, and inertial confinement fusion[11,35,39].

Over the past few decades, there have been several design iterations of LTDs with published experimental results[15,40–43]. However, based on the concept presented by Stygar et al.[1] in 2017 and prior to this paper, scientific publications have yet to exist for a successfully engineered and tested IMG as a next-generation pulsed-power driver. Fuse Energy Technologies (Fuse) has designed, built, and tested the world's first high-energy and high-power IMG named "TITAN." Design parameters of TITAN, 6-stage experimental results in correlation with simulated results as well as engineering challenges and solutions associated with IMG technology are presented in this paper.

TITAN design

In this section, we will discuss design parameters for 14-stage and 6-stage TITAN, including the triggering and air delivery systems (ADS).

IMG module

TITAN is a 14-stage, 1-TW IMG module powered by 238 bricks. Each brick consists of a pair of double-ended, 80-nF, 100-kV capacitors that are electrically connected in series through a normally open, pressurized, 200-kV field-distortion-triggered gas switch (FDGS). FDGS is a three-electrode gas switch which consists of two electrodes and a midplane that sits between them. One of the capacitors in a brick is charged to +100-kV and the other to −100-kV, such that a potential difference of 200-kV appears between the FDGS electrodes. Each brick has a maximum energy and power of 800-J and ~ 5-GW, respectively, and its LC time constant is designed to be ~ 80-ns. Each of the fourteen stages of TITAN is powered by seventeen identical bricks that are distributed azimuthally and connected in parallel, and the fourteen stages are electrically connected in series as a voltage adder (VA). In total, the energy storage capacitor bank of TITAN consists of 476 capacitors and 238 FDGSs organized into 238 identical bricks.

Due to the high-voltage operation (MV-scale) of TITAN, proper electrical isolation is critical to prevent arcs and surface discharges in all connections and parts. To achieve proper electrical isolation, the bricks are fully immersed in oil, and the space between the inner and outer conductors is filled with continuously recirculated, > 18-MΩ-cm deionized water. For efficient energy delivery, synchronized triggering of all FDGSs within the module at the speed of light is essential.

We have developed an idealized RLC circuit model of TITAN using the SCREAMER and LTspice circuit codes shown in Fig. 1a. In this model we assumed that all seventeen bricks within a stage are triggered simultaneously. In all RLC schematics, component subscripts "b," "s," and "T" stand for "brick," "stage," and "TITAN Module," respectively.

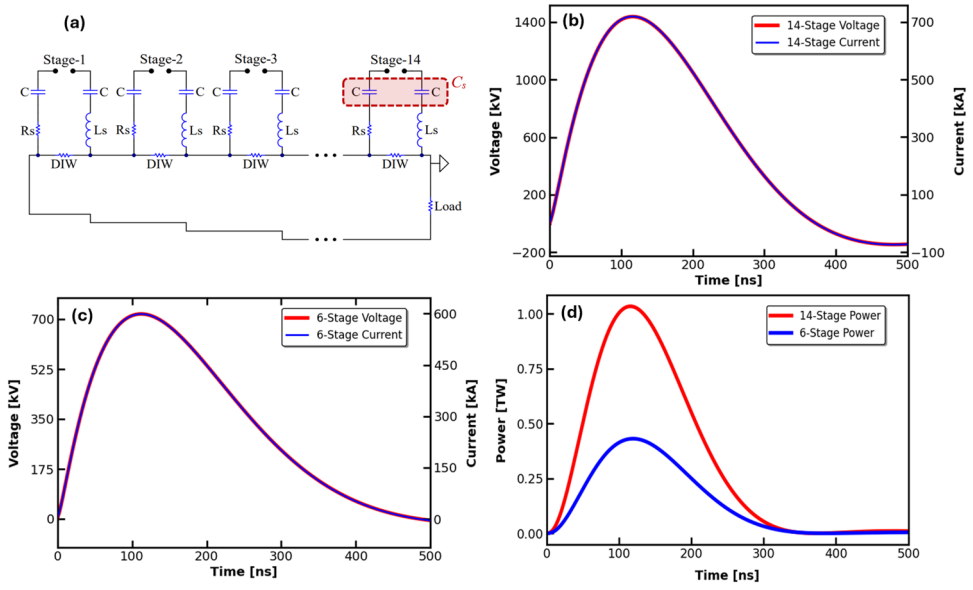

Figure 1. (**a**) Idealized RLC circuit model of 14-stage TITAN; "DIW" stands for deionized water. (**b**) Simulated voltage and current of 14-stage TITAN using LTspice (**c**) Simulated voltage and current of 6-stage TITAN (**d**) Simulated power-time histogram of 6-stage and 14-stage TITAN.

The capacitance of a single brick is $C_b = 40\text{-}nF$, and we assume the inductance and resistance of each brick to be $L_b = 160\text{-}nH$ and $R_b = 0.3\text{-}\Omega$, respectively. Using these values, we can calculate the LC time constant of a brick using Eq. (1):

$$\tau_b = \sqrt{L_b C_b} = 80\text{-}ns \tag{1}$$

Energy of a single brick can be calculated using Eq. (2), as follows:

$$U_b = 1/2 C_b V_b^2 = 800\text{-}J \tag{2}$$

TITAN is powered by 238 identical bricks which results in a total stored energy of $U_T = 190.4\text{-}k\text{J}$.
The impedance of a brick[13] can be calculated using Eq. (3):

$$Z_b = 1.1\sqrt{L_b/C_b} + 0.8R_b \approx 2.44\text{-}\Omega \tag{3}$$

As previously stated, TITAN has fourteen stages, $n_s = 14$, and each stage is powered by seventeen bricks, $n_b = 17$, which are electrically connected in parallel. Therefore, the impedance of a single stage "Z_s" can be calculate using Eq. (4):

$$Z_s = Z_b/n_b \approx 0.14\text{-}\Omega \tag{4}$$

Since the fourteen stages of TITAN are electrically connected in series, the impedance of a full TITAN module can be calculated using Eq. (5):

$$Z_T = n_s Z_s \approx 2\text{-}\Omega \tag{5}$$

As suggested by Spielman et al.[44], we have intentionally designed TITAN to be a 2-Ω IMG such that sixteen TITAN modules connected in parallel have the potential to make an intermediate pulsed-power facility Fuse plans to build called "Z-Star." Z-Star will be able to deliver a ~ 12-MA current and > 15-TW power to its matched load which is very similar to the impedance of the Z pulsed-power facility at SNL, $Z_{Z-Star} = Z_{Z-facility} = 0.125\text{-}\Omega$.

Based on the circuit model presented in Fig. 1a, simulated output voltage and current of 14-stage TITAN charged to ± 100-kV were plotted and are shown in Fig. 1b. As seen in Fig. 1b, TITAN can generate > 700-kA and > 1.4-MV on its 2-Ω impedance-matched load.

With the objective of risk-reduction in a fast, but credible and efficient manner, we chose to test all TITAN subcomponents such as the triggering, oil-delivery, deionized water, air delivery, charge & dump, and safety & interlock systems, as well as resistors and inductors, with six stages of TITAN first. Simulated output voltage and current for 6-stage TITAN charged to ± 100-kV are shown in Fig. 1c. As seen in Fig. 1c, 6-stage TITAN can generate ~ 600-kA and ~ 700-kV on its ~ 0.9-Ω matched load. The simulated peak powers generated by both 14-stage and 6-stage TITAN are shown in Fig. 1d.

Triggering system

Different LTD modules require different triggering technologies and types of trigger coupling between bricks. The CESZAR trigger circuit is equipped with an 80-nF capacitor bank that is used to trigger twenty FDGSs within a single LTD cavity. A 990-Ω resistive coupling is applied between trigger busbars and trigger pins[43]. Alternatively, an extendable triggering system was introduced for the M-50 testbed LTD module and achieved less than 2-ns jitter. Each unit of the extendable system has four PFLs to compress the triggering pulse and four laser triggered gas switches (LTGS). To achieve the desired waveform in M-50, all switches inside the LTD cavities must be triggered externally[25]. A different triggering system was used in BLUE, where a single-stage LTD cavity was equipped with 200-kV, Model 40264-200 kV FDGSs made by L3Harris. To amplify the trigger pulse, minimize the jitter of the switches, and isolate the switches from the breakdown process, inductive coupling was applied between the main trigger bus line and the UV-pins/midplanes of the switches[42].

The greatest challenge with LTD triggering is that each switch must be triggered externally. LTDs cannot run in a self-triggering mode without additional external trigger circuits coupled to all switches. Cavities in LTDs, unlike stages in IMGs, have individual separate enclosures, and the switches in one cavity are isolated from those in the other cavities. As a result, every single switch needs to be independently triggered[14], whereas in IMGs, as demonstrated in our experiments, only a few stages need independent triggering, and the other switches are self-triggered. In larger IMG-based, Petawatt-scale facilities, the difference is 100,000s of switches not needing external triggering.

To successfully trigger TITAN, we applied a triggering sequence described hereafter that achieves the maximum efficiency of the triggering system. The TITAN triggering system starts with an 8-Channel digital delay generator (DDG), model DG645, manufactured by Stanford Research Systems. The DDG on a transistor–transistor logic (TTL) circuit drives a pulse-generator (PG) unit which generates 35-kV with a 200-ns rise time. The PG then drives a fast, compact trig generator (TG) which can generate a 40-kV pulse with a 10–90% rise time of 4-ns. The TG delivers its signal through a single 59-Ω, 15-ns transmission line (TL) to two identical, compact, low-inductance Marx generators called "BFMGs." A BFMG is a 4-stage, coaxial Marx generator that can generate a > 150-kV pulse with a 10–90% rise time of ~ 13-ns when charged to 30-kV. TITAN uses two BFMGs to trigger stage-1, 2, and 3. BFMG-I has four channels that deliver trigger-pulse-1 to stage-1 through four 59-Ω, ~ 45-ns TLs, and BFMG-II has eight channels that deliver trigger-pulse-2 to stage-2 through four 59-Ω, ~ 54-ns TLs and trigger-pulse-3 to stage-3 through four 59-Ω, ~ 63-ns TLs. Distribution of the trigger pulse at stage-1 is presented in Fig. 2a. All switch midplanes within a single, non-triggered stage are coupled through 2-μH inductors. The

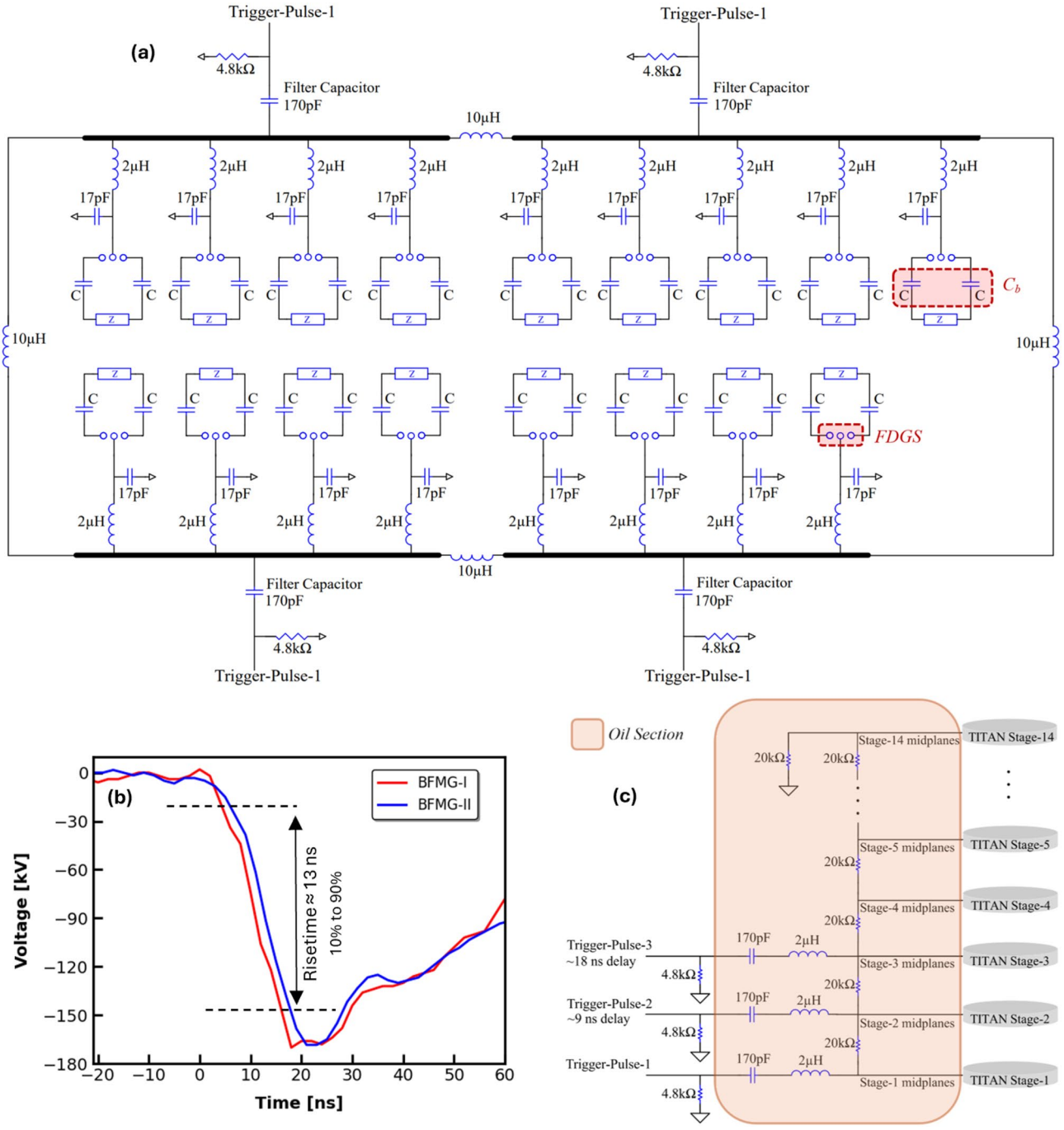

Figure 2. (**a**) Distribution of the trigger pulse in the first stage of TITAN (**b**) BFMG-I and BFMG-II voltage signals with ~ 2-ns jitter, ~ 13-ns risetime (**c**) Distribution of the trigger pulse between TITAN stages.

two BFMGs are isolated from each other by two 100-Ω resistors. As seen in Fig. 2b the measured output jitter between the two BFMGs is ~ 2-ns. As shown in Fig. 2c, FDGS midplanes for every stage are isolated from nearby stages by 20-kΩ HV resistors in the oil section, and the last stage midplane is grounded through a 20-kΩ HV resistor. All triggering subsystems, including PG, TG, and BFMGs, are developed by Fuse.

One of the biggest unforeseen challenges in IMG engineering is isolating the triggering TLs from the triggering midplanes. During a shot, the first three triggering stages of TITAN will rise to 300-kV < $V_{Midplanes}$ < 1000-kV, which drives the need for triggering cables to be isolated from the high voltage midplanes. Conventional Marx generators are triggered from the stages furthest from the load, whereas TITAN is triggered from the stages closest to the load (we have called those stages-1, 2, and 3 in our design). The maximum voltage present in the module appears in the closest stages to the load where the external triggering system is connected. When 14-stage TITAN is charged to ± 70-kV, after the system is triggered, stage-1 (the stage closest to the load) will see a potential

of $V = 14 \times 70 \sim 1000$-kV. This high voltage will be seen across the midplanes of the switches connected to the trigger system. Thus, we must isolate the triggering transmission lines from that voltage to protect the circuit.

There are two different methods that have the potential to solve this problem. The first method is to add a HV resistor in series with the triggering TL, and to connect this resistor to the midplane. The capacitance of the midplane in one of TITAN's FDGSs is ~ 17-pF. By adding a 2-kΩ HV resistor, the charging time of the midplane capacitor would increase to ~ RC which is ~ 34-ns. Clearly, this method would slow down the trigger pulse of TITAN which is not ideal. Furthermore, this resistor must withstand 1000-kV, requiring its inductance to be high and its size to be big. In this case, the use of a water/liquid/aqueous resistor is suggested, however, that would require a regular maintenance plan.

The second method is to apply a 1000-kV filter capacitor as a high-pass filter at the output tip of the triggering TLs. We have applied this solution to TITAN and made twelve 170-pF, 1000-kV filter capacitors, as shown in Fig. 2a and c. The capacitors are placed within the oil section of the module to insulate them from TITAN's triggering system. Unlike resistors, these filter capacitors are maintenance-free and do not slow down the triggering pulse, offering a major advantage both mechanically and electrically.

Air delivery system (ADS)

As mentioned earlier, 14-stage and 6-stage TITAN are powered by 238 bricks/FDGSs and 102 bricks/FDGSs, respectively, and all switches operate under pressurized conditions, similar to LTDs[41]. In every LTD module, all switches operate under equal air pressure. As with LTD modules, an IMG module needs an air delivery system. NGPP facilities will be powered by more than 100,000 bricks and FDGSs, and there are two major challenges that arise concerning this large quantity of gas switches: The first is reducing the switches' pre-fire rate, and the second is pulse shaping. To overcome these challenges, we have designed an air delivery system (ADS) for TITAN such that the pressure within the gas switches in each stage can be controlled independently. There are three main advantages of this novel design:

I. We can pressurize the triggering stages of TITAN (stage-1, 2, and 3) to the specific pressure required to achieve the minimum jitter, while simultaneously applying higher pressure to the remaining switches to reduce the rate of pre-fire.
II. We can start stage-1 from a high pressure and gradually decrease the pressure in each successive stage to achieve the lowest possible pressure in the last stage. In this case, the rise time and length of the output pulse will increase (slow pulse, long pulse).
III. We can start stage-1 from a low pressure and gradually increase the pressure in each stage to achieve the highest pressure in the last stage. In this case, the rise time and length of the output pulse will decrease (fast pulse, short pulse).

Each of the three novel concepts mentioned above have been experimentally tested and proven in TITAN, and they are discussed in the experimental results section of this paper. To control the pressures across all fourteen stages, TITAN makes use of a unique ADS. The main function of the ADS is to supply Ultra 0 Grade Dry Air to the FDGSs while allowing for independent pressure control of each TITAN stage within the range of 0 to 6.9×10^5-Pa (0 to 100-psig) ± 1%. Increasing the pressure within a stage increases the minimum breakdown voltage required to trigger the stage. Refreshing the gas across all stages follows a 4-step procedure:

I. Venting the high pressure from the previous experimental shot.
II. Vacuuming any residual air and sputtered particles within the FDGSs to -6.9×10^4-Pa (-10-psig).
III. Flowing fresh gas continuously through the switches.
IV. Filling the stages to the desired pressure level.

This 4-step process is fully automated on TITAN using Fuse proprietary technology. Figure 3a shows a simplified schematic of the TITAN ADS. Furthermore, the 3D model of TITAN, including its wire array implosion (WAI) load stalk, is presented in Fig. 3b. Every stage is divided into three gas sectors to improve the speed and quality of the gas-refreshing process. The pressure on each stage is controlled with an electro-pneumatic regulator, and data is captured with a pressure transmitter. The use of Ultra 0 Grade Dry Air in the FDGSs instead of SF_6-filled switches, eliminates the usage of a toxic and green-house-gas emitting gas.

Experimental results and discussion

In this section, the experimental results of 6-stage TITAN are presented. The experiments were aimed at characterizing the output current, voltage, and power waveforms of the IMG, comparing those measurements to simulated results using SCREAMER, and establishing pulse shaping possibilities under varying stage pressure operating conditions.

An overview of the experimental setup and methodology employed to estimate the inductance of a single TITAN brick, as well as its measured and simulated current waveforms, are presented first. Following that, measured current, voltage, and power waveforms and their agreement with simulated results for experimental tests of 6-stage TITAN are presented. Synchronization of triggering within the stages and the repeatability of TITAN's experimental results are included in the evaluation of the device's performance. Finally, the discovery of pulse-shaping capabilities using a novel concept of varying gas-switch fill pressures between each of the stages of 6-stage TITAN is discussed.

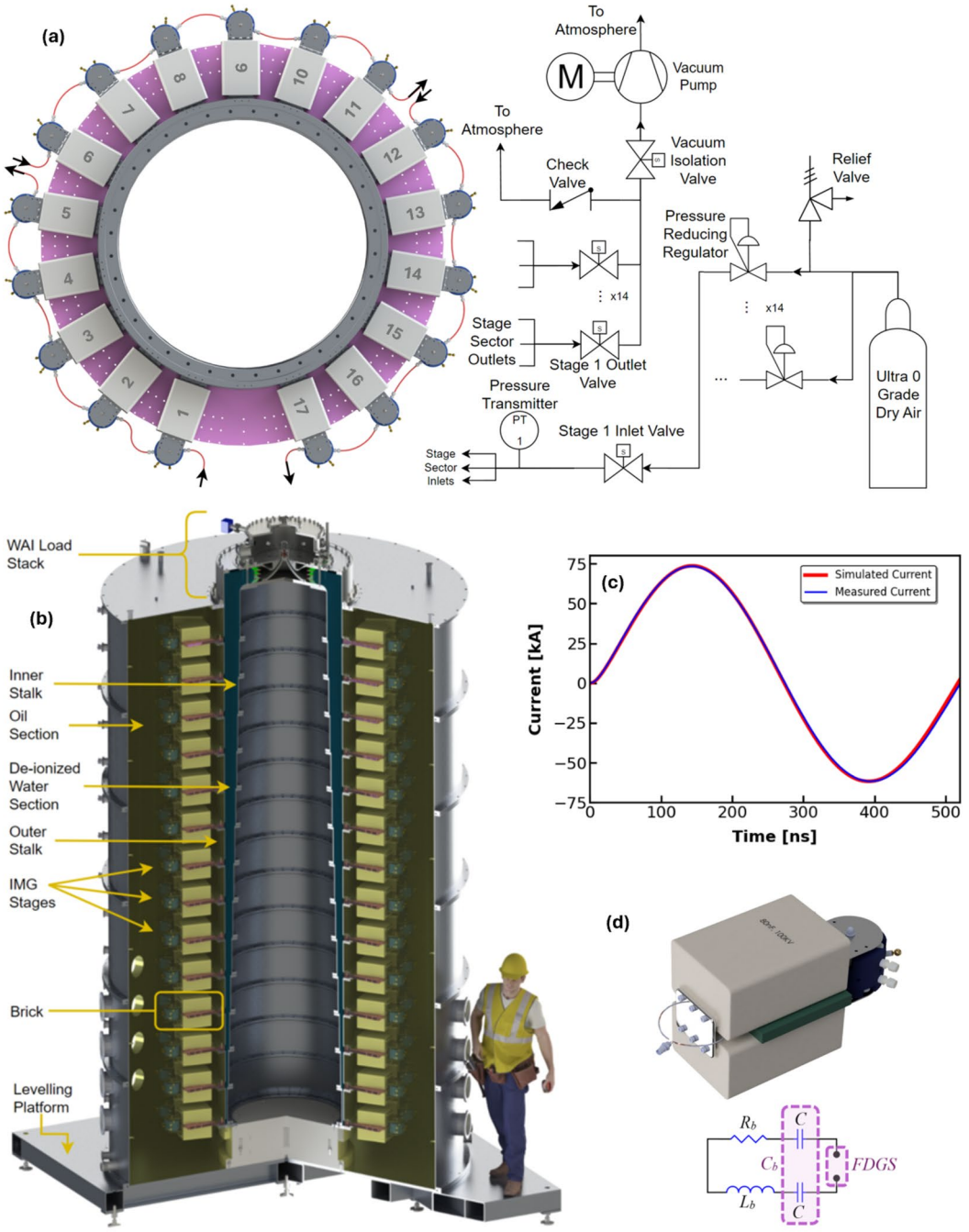

Figure 3. (**a**) TITAN ADS piping and instrumentation diagram (**b**) 3D model of 14-stage TITAN including its WAI load stack. It consists of ~ 40,000 parts, ~ 20,000 L oil, and ~ 640 L of deionized water, and it weighs ~ 22 tons. (**c**) Measured and simulated current of TITAN's single brick discharge at ± 85-kV, 4.8 × 10^5-Pa (70-psig). (**d**) 3D model of TITAN's brick and its equivalent circuit.

Brick test

As explained in "TITAN design" section, a brick consists of two capacitors and an L3Harris, model 50264, FDGS. Figure 3d shows a 3D model of a brick test setup and its equivalent electrical circuit. The test was designed to evaluate the inductance of a single brick of TITAN.

The brick capacitors were submerged in oil and charged to ± 85-kV, and the FDGS was pressurized to 4.8 × 10^5 -Pa (70-psig). The brick discharge current was measured using a Rogowski coil. The current waveform from the brick test is shown in Fig. 3c. Analysis of the measurement demonstrated that the best fit between simulated and experimental waveforms was achieved when $L_b = 150\text{-}nH$.

6-Stage

Each stage of TITAN has seventeen bricks connected in parallel, and each of the stages are connected to one another in series. 6-stage TITAN is comprised of 102 bricks charged up to ± 70-kV and uses a resistive load for discharging. To charge the bricks, two power supplies (one negative and one positive) are connected to stage-6, and two parallel 200-k Ω, 200-kV resistors are placed between the stages to allow each capacitor to be charged from stage-6 down to stage-1. The resistive load for discharging is composed of three 3.6-Ω ± 10%, 990-kJ, oil-saturated, high-energy, HV disc resistors from HVR advanced power components, Inc (I09PDA3R6k).

Experimental results for the discharge current, voltage, and power waveforms are shown in Fig. 4. During these experiments, the FDGS fill pressure was 3.8×10^5-Pa (55-psig) for all switches, the bricks were charged to ± 50-kV, and the bricks were discharged through a 1.2-Ω resistive load (three 3.6-Ω in parallel). Current waveforms were measured using a Pearson current probe that was situated around a known inductor at the ground side of one of the resistors. The current, voltage, and power waveforms were analyzed and compared with the SCREAMER equivalent circuit simulation results. As seen in Fig. 4a and b, the measured peak current, peak voltage, and peak power for a ± 50-kV brick charging voltage were 378-kA, 454-kV, and 171-GW, respectively. These measurements closely align with their SCREAMER simulation counterparts, which yielded peak current, peak voltage, and peak power readings of 381-kA, 457-kV, and 174-GW, respectively. The maximum error between measured and simulated values is < 1%. This agreement between simulated and experimental results is presented in Fig. 4a and b. Repeatability of the experimental waveform is shown in Fig. 4c, where 5 consecutive shots are compared.

The synchronized triggering of intra-stage switches was monitored using five Silicon Photomultipliers (SiPMs). These sensors were positioned as follows: one in stage-1 on brick number 6, two in stage-3 on the 6th and 17th bricks, and two in stage-6 on the 6th and 17th bricks as labeled in Fig. 3a. The experimental waveforms from the SiPMs are shown in Fig. 4d and demonstrate TITAN's highly synchronized triggering. As presented in Fig. 4d, the measured triggering delay between stages is larger than the electromagnetic wave transit time between the stages. More investigation and experimental results are required to solidify the reasoning for this delay and its impact on impedance matching.

In these experiments, 6-stage TITAN was tested up to a ± 70-kV charge voltage which delivers a peak power of 330-GW to its 1.2-Ω resistive load, as shown in Fig. 5a.

To reduce the pre-fire rate and achieve minimal intra-stage jitter at high operating voltages, the first three stages of TITAN were pressurized to a given level, while a slight (~ 9%) increase in pressure was applied to the remaining stages.

Pulse shaping

One of the novel experiments conducted with 6-stage TITAN was pulse shaping due to varying the inter-stage FDGS fill pressures. As mentioned in section "TITAN Design", TITAN's ADS was designed such that the fill pressure of the FDGSs in each stage could be independently controlled. To test the concept of shaping the pulse

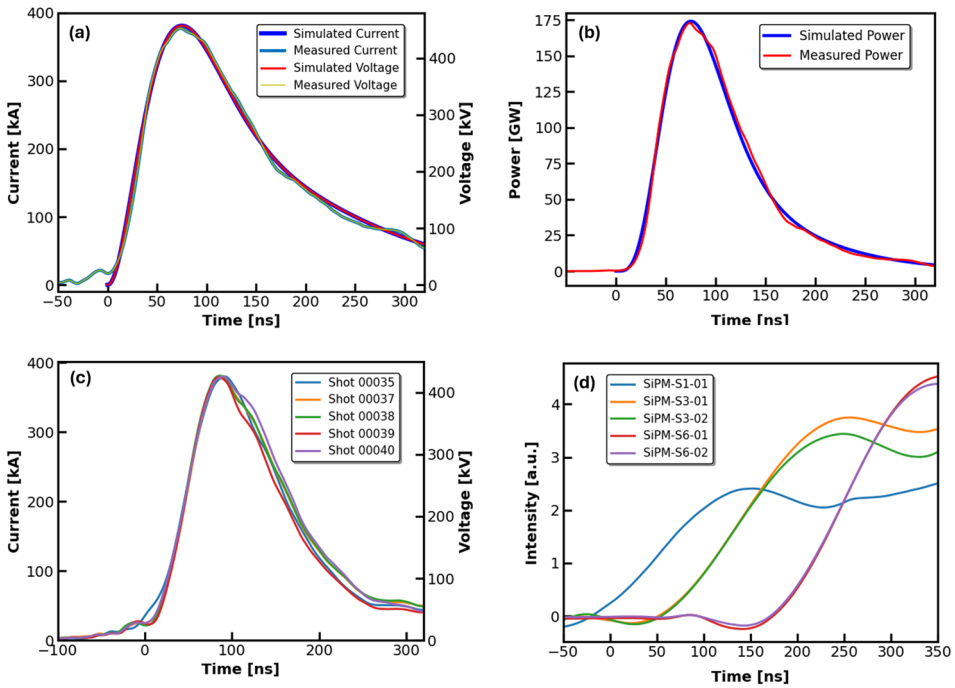

Figure 4. (**a**) Measured and simulated current and voltage of 6-stage TITAN at ± 50-kV. (**b**) Measured and simulated output power of 6-stage TITAN at ± 50-kV. (**c**) Repeatability of the waveforms for five consecutive shots at ± 50-kV. (**d**) Synchronized triggering of intra-stage switches monitored using five SiPMs.

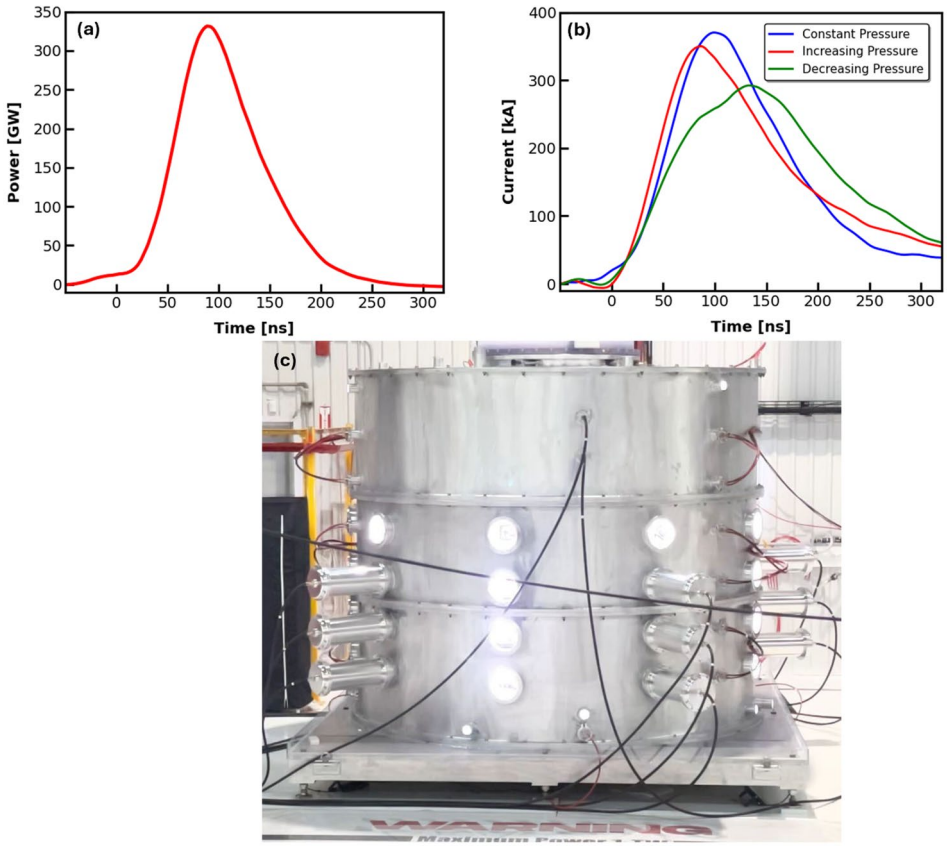

Figure 5. (**a**) Measured peak power of 6-stage TITAN at ± 70-kV. (**b**) Pulse shaping capability of 6-Stage TITAN at ± 50-kV. (**c**) 6-stage TITAN during a shot captured by a fast camera.

by varying the gas pressure of the switches between stages, experiments were conducted under the following three scenarios:

I. Constant pressure: All bricks in every stage are filled to the same pressure of 3.8×10^5-Pa (55-psig).
II. Increasing pressure: The initial three stages (stage-1, 2, and 3) are maintained at a fill pressure of 3.8×10^5-Pa (55-psig), and each successive stage is filled with an additional 3.4×10^4-Pa (5-psig). Stage-4, 5, and 6 have 4.1×10^5-Pa (60-psig), 4.5×10^5-Pa (65-psig), and 4.8×10^5-Pa (70-psig), respectively.
III. Decreasing pressure: The initial three stages (stage-1, 2, and 3) are maintained at a fill pressure of 4.8×10^5-Pa (70-psig), each successive stage is filled with a reduction of 3.4×10^4-Pa (5-psig). Stage-4, 5, and 6 have 4.5×10^5-Pa (65-psig), 4.1×10^5-Pa (60-psig), and 3.8×10^5-Pa (55-psig), respectively.

The effect that adjusting inter-stage pressures had on the shape of the pulse is depicted in Fig. 5b. Increasing the fill pressure of the upper stages (Scenario II) yielded shorter rise times and reduced Full Width at Half Maximums (FWHM), whereas reducing their fill pressure (Scenario III) led to longer rise times and larger FWHMs. The measured rise times for Scenarios I, II, and III were 99.2-ns, 83.6-ns, and 128.2-ns, respectively; and the FWHM values were observed to be 130-ns, 125-ns, and 181-ns, respectively. 6-stage TITAN during a shot captured by a fast camera is presented in Fig. 5c.

Conclusion

Impedance-matched Marx generators are the next-generation pulsed-power drivers because of their long lifetime (> 10,000 shots), repeatability (> 0.1-Hz), fast rise time (~ 100-ns), and high energy delivery efficiency (~ 90%). In this paper, design parameters of a 14-stage, 1-TW, and 2-Ω impedance-matched Marx generator called "TITAN" were presented. TITAN consists of > 40,000 parts, ~ 20,000 L of oil, and 640 L of continuously recirculating deionized water, and it weighs ~ 22 tons. The 6-stage TITAN testbed is powered by 102 identical bricks and field distortion gas switches, and it has the potential to generate ~ 600-kA and ~ 700-kV on a ~ 0.9-Ω matched load when fully charged to ± 100-kV. In these experiments, 6-stage TITAN was tested up to ± 70-kV charge voltage which consistently delivered a peak power of 330-GW to its 1.2-Ω resistive load. The experimental results correlate with the simulated results with > 99% accuracy.

One of the biggest challenges in IMG engineering is isolating the triggering transmission lines from the triggering midplanes. To accomplish this, twelve 170-pF, 1000-kV high-pass filter capacitors were placed within the oil section of TITAN, insulating the midplanes from TITAN's trigger system.

The midplanes of the seventeen bricks at each stage were connected through seventeen 2-μH inductors, and each stage was coupled to the next using a 20-kΩ HV resistor. Five SiPM sensors positioned at stage-1, 3, and 6 have recorded synchronized triggering within the individual stages.

To reduce the pre-fire rate of TITAN, and to achieve pulse shaping capabilities in the module, an air delivery system has been designed to supply Ultra 0 Grade Dry Air to the gas switches while providing independent pressure control of each stage over a range of 0 to 6.9×10^5-Pa (0 to 100-psig) ± 1%. By gradually increasing the gas pressure within the switches from stage-1 to stage-6, the module was able to generate fast pulses with a ~ 80-ns rise time. Conversely, by gradually decreasing the gas pressure within the switches from stage-1 to stage-6, the module was able to generate slow pulses with a ~ 130-ns rise time. The use of Ultra 0 Grade Dry Air in the FDGSs, instead of SF_6-filled switches, eliminates the usage of a toxic and green-house-gas emitting gas.

More experimental results will be presented when all 14 stages of TITAN are assembled. In particular, the pulse-shaping capabilities of 14-stage TITAN are expected to be even greater than what has been discovered with 6-stages. The ability to alter the rise time between all 14 stages allows for even more control over the shape of the pulses produced. 14-stage TITAN is expected to deliver 1-TW of power to its 2-Ω matched load.

Data availability

Data sets generated during the current study are available from the corresponding author on reasonable request.

Received: 14 May 2024; Accepted: 15 July 2024
Published online: 23 July 2024

References

1. Stygar, W. A. *et al.* Impedance-matched Marx generators. *Phys. Rev. Accel. Beams* **20**, 040402 (2017).
2. Stygar, W. *et al.* Conceptual design of a 960-TW accelerator powered by impedance-matched Marx generators. In *2017 IEEE 21st International Conference on Pulsed Power (PPC)* 1–8 (IEEE, 2017). https://doi.org/10.1109/PPC.2017.8291256.
3. van Oorschot, J. J. & Huiskamp, T. Fast and flexible, arbitrary waveform, 20-kV, solid-state, impedance-matched Marx generator. *IEEE Trans. Plasma Sci.* **51**, 560–571 (2023).
4. Guegan, B., Bayol, F., Arnal, D. & Mouly, P. Mega-volt impedance-matched Marx. In *2021 IEEE Pulsed Power Conference (PPC)* 1–6 (IEEE, 2021). https://doi.org/10.1109/PPC40517.2021.9733131.
5. Huiskamp, T. & Van Oorschot, J. J. Fast pulsed power generation with a solid-state impedance-matched Marx generator: Concept, design, and first implementation. *IEEE Trans. Plasma Sci.* **47**, 4350–4360 (2019).
6. Lee, S., Damideh, V. & Btaiche, J. C. MagLIF: Dynamics and energetics of liner and fuel. *Vacuum* **216**, 112471 (2023).
7. Wurden, G. A. *et al.* Magneto-inertial fusion. *J. Fusion Energy* **35**, 69–77 (2016).
8. Yager-Elorriaga, D. A. *et al.* An overview of magneto-inertial fusion on the Z machine at Sandia National Laboratories. *Nuclear Fusion* **62**, 042015 (2022).
9. Gomez, M. R. *et al.* Performance scaling in magnetized liner inertial fusion experiments. *Phys. Rev. Lett.* **125**, 155002 (2020).
10. Awe, T. J. *et al.* Observations of modified three-dimensional instability structure for imploding Z-pinch liners that are premagnetized with an axial field. *Phys. Rev. Lett.* **111**, 235005 (2013).
11. LeChien, K. R. *et al. Sirius I: Prototype of a Prime-Power Source for Future 1 - 10 GJ Fusion-Yield Experiments.* (2023).
12. Sinars, D. B. *et al.* Review of pulsed power-driven high energy density physics research on Z at Sandia. *Phys. Plasmas* **27**, 070501 (2020).
13. Stygar, W. A. *et al.* Architecture of petawatt-class z-pinch accelerators. *Phys. Rev. Spec. Top. Accel. Beams* **10**, 030401 (2007).
14. Stygar, W. A. *et al.* Conceptual designs of two petawatt-class pulsed-power accelerators for high-energy-density-physics experiments. *Phys. Rev. Spec. Top. Accel. Beams* **18**, 110401 (2015).
15. Douglass, J. D. *et al.* Experimental Results from the 1.2 ma, 2.2 m Diameter Linear Transformer Driver at Sandia National Labs. In *2019 IEEE Pulsed Power & Plasma Science (PPPS)* 1–5 (IEEE, 2019). https://doi.org/10.1109/PPPS34859.2019.9009908.
16. Damideh, V. *et al.* Characteristics of Fast ion beam in Neon and Argon filled plasma focus correlated with Lee Model Code. *Vacuum* **169**, 108916 (2019).
17. Auluck, S. *et al.* Update on the scientific status of the plasma focus. *Plasma* **4**, 450–669 (2021).
18. Gribkov, V. A. *et al.* Plasma dynamics in the PF-1000 device under full-scale energy storage: II. Fast electron and ion characteristics versus neutron emission parameters and gun optimization perspectives. *J. Phys. D Appl. Phys.* **40**, 3592–3607 (2007).
19. Schmidt, A. *et al.* First experiments and radiographs on the MegaJOuLe neutron imaging radiography (MJOLNIR) dense plasma focus. *IEEE Trans. Plasma Sci.* **49**, 3299–3306 (2021).
20. Engelbrecht, J. T. *et al.* Initial conditions in the hawk dense plasma focus. In *2019 IEEE Pulsed Power & Plasma Science (PPPS)* 1–5 (IEEE, 2019). https://doi.org/10.1109/PPPS34859.2019.9009625.
21. Avaria, G. *et al.* Bayesian inference of spectrometric data and validation with numerical simulations of plasma sheath diagnostics of a plasma focus discharge. *Sci. Rep.* **12**, 15601 (2022).
22. Sohrabi, M., Zarinshad, A. & Habibi, M. Breakthrough in 4π ion emission mechanism understanding in plasma focus devices. *Sci. Rep.* **6**, 38843 (2016).
23. David L. Smith, M. E. S. ZR Marx capacitor lifetime test results. In *Conference Record of the Twenty-Sixth International Power Modulator Symposium, 2004 and 2004 High-Voltage Workshop.* 530–533 (IEEE). https://doi.org/10.1109/MODSYM.2004.1433631.
24. Savage, M. E. *et al.* Pulsed power performance of the Z machine: Ten years after the upgrade. In *2017 IEEE 21st International Conference on Pulsed Power (PPC)* 1–6 (IEEE, 2017). https://doi.org/10.1109/PPC.2017.8291252.
25. Chen, L. *et al.* Development of a fusion-oriented pulsed power module. *Phys. Rev. Accel. Beams* **22**, 030401 (2019).
26. Owens, I. *et al.* Electro-optical measurement of intense electric field on a high energy pulsed power accelerator. *Sci. Rep.* **11**, 10702 (2021).
27. Hadjisolomou, P., Jeong, T. M. & Bulanov, S. V. Towards bright gamma-ray flash generation from tailored target irradiated by multi-petawatt laser. *Sci. Rep.* **12**, 17143 (2022).
28. Esplen, N. *et al.* Dosimetric characterization of a novel UHDR megavoltage X-ray source for FLASH radiobiological experiments. *Sci. Rep.* **14**, 822 (2024).
29. Venkata Ramudu, B., Reddy, C. J. & Madhu, V. Flash X-ray radiography technique to study the high velocity impact of soft projectile on E-glass/epoxy composite material. *Defence Technol.* **15**, 216–226 (2019).
30. Obenschain, S. *et al.* High-energy krypton fluoride lasers for inertial fusion. *Appl. Opt.* **54**, F103 (2015).

31. Nowak, M. The concept of a new two-stage fuse for high power pulse forming. *Sci. Rep.* **12**, 18176 (2022).
32. Bhartiya, P. *et al.* Pulsed 3.5 GHz high power microwaves irradiation on physiological solution and their biological evaluation on human cell lines. *Sci. Rep.* **11**, 8475 (2021).
33. Lu, Y. *et al.* A compact platform for the investigation of material dynamics in quasi-isentropic compression to ~19 GPa. *Sci. Rep.* **11**, 20688 (2021).
34. Pascarelli, S. *et al.* Materials under extreme conditions using large X-ray facilities. *Nat. Rev. Methods Primers* **3**, 82 (2023).
35. Zylstra, A. B. *et al.* Burning plasma achieved in inertial fusion. *Nature* **601**, 542–548 (2022).
36. Faenov, A. Y. *et al.* Advanced high resolution x-ray diagnostic for HEDP experiments. *Sci. Rep.* **8**, 16407 (2018).
37. Valenzuela, J. C. *et al.* Measurement of temperature and density using non-collective X-ray Thomson scattering in pulsed power produced warm dense plasmas. *Sci. Rep.* **8**, 8432 (2018).
38. Min, S.-H. *et al.* Effects on electronics exposed to high-power microwaves on the basis of a relativistic backward-wave oscillator operating on the X-band. *J. Electromagn. Waves Appl.* **31**, 1875–1901 (2017).
39. Mehlhorn, T. A. National security research in plasma physics and pulsed power: Past, present, and future. *IEEE Trans. Plasma Sci.* **42**, 1088–1117 (2014).
40. Kim, A. A. *et al.* Development and tests of fast 1-MA linear transformer driver stages. *Phys. Rev. Spec. Top. Accel. Beams* **12**, 050402 (2009).
41. LeChien, K. *et al.* A 1-MV, 1-MA, 0.1-Hz linear transformer driver utilizing an internal water transmission line. In *2009 IEEE Pulsed Power Conference* 1186–1191 (IEEE, 2009). https://doi.org/10.1109/PPC.2009.5386430.
42. Sporer, B. J. *et al.* Multicavity linear transformer driver facility for z-pinch and high-power microwave research. *Phys. Rev. Accel. Beams* **24**, 100402 (2021).
43. Conti, F. *et al.* MA-class linear transformer driver for z-pinch research. *Phys. Rev. Accel. Beams* **23**, 090401 (2020).
44. Spielman, R. B. *et al.* Conceptual design of a 15-TW pulsed-power accelerator for high-energy-density–physics experiments. *Matter Radiat. Extrem.* **2**, 204–223 (2017).

Author contributions

Supervision, writing, review and editing, V.D.; resources, writing, review and editing, J.C.B.; validation, review and editing, A.H., R.B.S., J.M.L. and T.A.M.; writing, original draft preparation, data analysis, simulation, I.H.; writing, original draft preparation, A.A.; writing, original draft preparation, simulation, E.A.; technical support, A.M., P.T., A.C., and E.B.; data acquisition, H.X.T. and A.Y.; writing, original draft preparation, simulation, S.F.; technical support, R.T., G.B., R.T., N.H., and E.S. All authors have read and agreed to the published version of the manuscript.

Competing interests

The authors declare no competing interests.

Additional information

Correspondence and requests for materials should be addressed to V.D.

Reprints and permissions information is available at www.nature.com/reprints.

Publisher's note Springer Nature remains neutral with regard to jurisdictional claims in published maps and institutional affiliations.